Articular cartilage response to a sliding load using two different-sized spherical indenters

Schätti, Oliver R ; Colombo, Vera ; Torzilli, Peter A ; Gallo, Luigi Maria

Abstract: BACKGROUND: Cartilage surface contact geometry influences the deformational behavior and stress distribution throughout the extracellular matrix (ECM) under load. OBJECTIVE: To test the correlation between the mechanical and cellular response of articular cartilage when loaded with two different-sized spherical indenters under dynamic reciprocating sliding motion. METHODS: Articular cartilage explants were subjected to a reciprocating sliding load using a 17.6 mm or 30.2 mm spherical ball for 2000 cycles at 10 mm/s and 4 kg axial load. Deformation of the cartilage was recorded and contact parameters were calculated according to Hertzian theory. After mechanical loading cartilage samples were collected and analyzed for ECM collagen damage, gene regulation and proteoglycan (PG) loss. RESULTS: Significantly higher ECM deformation and strain and lower dynamic effective modulus were found for explants loaded with the smaller diameter indenter whereas contact radius and stress remained unaffected. Also, the 17.6 mm indenter increased PG loss and significantly upregulated genes for ECM proteins and enzymes as compared to the 30.2 mm indenter. CONCLUSION: Sliding loads that increase ECM deformation/strain were found to induce enzyme-mediated catabolic processes in articular cartilage explants. These observations provide further understanding of how changes in cartilage contact mechanics under dynamic conditions can affect the cellular response.

DOI: https://doi.org/10.3233/BIR-16110

ARTICULAR CARTILAGE RESPONSE TO A SLIDING LOAD USING TWO DIFFERENT-SIZED SPHERICAL INDENTERS

Oliver R. Schätti, PhD [a,b,c]
Vera Colombo, PhD [b*]
Peter A. Torzilli, PhD [a]
Luigi M. Gallo, PhD [b]

[a] Laboratory for Soft Tissue Research, Hospital for Special Surgery, Street, New York, NY, USA
[b] Laboratory of Physiology and Biomechanics of the Masticatory System, Center for Oral Medicine, Dental and Maxillo-Facial Surgery, University of Zurich, Switzerland.
[c] Institute for Biomechanics, ETH Zürich, Switzerland.

Corresponding author:
Plattenstrasse 11, 8032 Zürich
Tel. +41 (0)44 634 33 53; fax: +41 (0)44 634 43 12
E-mail address: vera.colombo@zzm.uzh.ch

The work reported was done at the following institute:
Laboratory for Soft Tissue Research, Hospital for Special Surgery, 535 East 70th Street, New York, NY

Running Title: Dynamic Cartilage Mechanobiology

Keywords: Contact Mechanics, Indenter Size, Mechanobiology, Gene Regulation, Proteoglycan Loss

BACKGROUND: Cartilage surface contact geometry influences the deformational behavior and stress distribution throughout the extracellular matrix (ECM) under load.

OBJECTIVE: To test the correlation between the mechanical and cellular response of articular cartilage when loaded with two different-sized spherical indenters under dynamic reciprocating sliding motion.

METHODS: Articular cartilage explants were subjected to a reciprocating sliding load using a 17.6 mm or 30.2 mm spherical ball for 2000 cycles at 10 mm/s and 4 kg axial load. Deformation of the cartilage was recorded and contact parameters were calculated according to Hertzian theory. After mechanical loading cartilage samples were collected and analyzed for ECM collagen damage, gene regulation and proteoglycan (PG) loss.

RESULTS: Significantly higher ECM deformation and strain and lower dynamic effective modulus were found for explants loaded with the smaller diameter indenter whereas contact radius and stress remained unaffected. Also, the 17.6 mm indenter increased PG loss and significantly upregulated genes for ECM proteins and enzymes as compared to the 30.2 mm indenter.

CONCLUSION: Sliding loads that increase ECM deformation/strain were found to induce enzyme-mediated catabolic processes in articular cartilage explants. These observations provide further understanding of how changes in cartilage contact mechanics under dynamic conditions can affect the cellular response.

1. Introduction

From decades of research on the mechanical and biological responses of cartilage to various stimuli, it is clear that mechanical factors have considerable influence on cartilage health and disease [1–3]. Strains and stresses have long been identified as parameters influencing chondrocyte metabolism and extracellular matrix (ECM) integrity. Forces within a physiological range are associated with normal ECM turnover and an effort of the chondrocytes to adapt the ECM in response to the loading conditions [4,5]. On the other hand, non-physiological forces have been shown to lead to ECM damage that manifests itself in proteoglycan (PG) loss and collagen fiber disruption [6] and an increase in catabolic enzymes such as matrix metalloproteinases (MMPs) and disintegrin and metalloproteinase with thrombospondin motifs (ADAMTS') [7–10]. Also, the increase in other proteins that are associated with degenerative changes of the ECM have been reported, such as fibronectin and cartilage oligomeric matrix protein (COMP) [11–13]. How the chondrocytes within the cartilage ECM respond to mechanical forces, that is anabolic or catabolic biosynthesis, will depend on the magnitude of the strains and stresses within the ECM. Based on these described mechanism, we would expect that relative to the larger diameter indenter, the smaller indenter would cause increased surface fibrillation, increased enzyme gene expressions for MMP-3, MMP-13, ADAMTS-4 and ADAMTS-5, and increased protein gene expression for collagen type II, aggrecan, fibronectin and COMP. From biomechanical studies it is known that these parameters are functions of loading rate and duration and also the location-dependent mechanical properties of the ECM [14–17].

A further factor influencing contact mechanics and local ECM strains and stresses is the geometry of the contacting cartilage surfaces [18]. The two cartilage surfaces engaging in

relative motion are never perfectly congruent, and as a consequence geometrical differences will influence the deformational behavior and stress distribution throughout the ECM, ultimately influencing the mechanobiological response of the tissue. In fact, studies have shown that the degree of congruence between the opposing cartilage surfaces can influence cartilage contact parameters in the ECM, and even small variations in geometry can lead to significant changes in contact mechanics which have been correlated with osteoarthritis (OA)-related changes [18,19]. However, the vast majority of such studies were patient-specific and based on imaging techniques in combination with finite element models (FEM). While these data provide valuable epidemiological information, general information on how the mechanobiological reaction of articular cartilage to changing contact geometries during joint motion is difficult to obtain. A limited number of *in vitro* studies have analyzed the mechanical response of articular cartilage to different indenter curvatures under dynamic sliding loads. These found that by using spherical indenters the contact radius was a function of indenter curvature and sliding speed [20–22]. Hence, indenter shape and size are crucial factors governing the contact mechanics, and the change of either can lead to alterations in ECM strains and stresses. Thus, the aim of this study was to investigate the influence of indenter curvature (spherical radius) on contact mechanics (strains and stresses) during reciprocating sliding motion and how this affected the metabolic response of the chondrocytes evoked through changes in the mechanical environment.

We hypothesized that the application of a sliding load with a small diameter spherical indenter, compared to a large diameter spherical indenter, would result in increased cartilage damage, catabolic gene up-regulation and PG loss. We postulated that the main mechanical mechanisms for this mechanobiological response were due to the increased ECM strains and stresses that arise from the reduced contact area between the smaller diameter indenter and the

cartilage surface [23]. Based on this damage mechanism, we hypothesized that relative to the larger diameter indenter the smaller indenter would cause increased surface fibrillation, increased enzyme gene expressions for MMP-3, MMP-13, ADAMTS-4 and ADAMTS-5, and increased protein gene expression for collagen type II, aggrecan, fibronectin and COMP.

In order to test our hypotheses, we applied a dynamic reciprocating sliding load on the surface of articular cartilage explants using two different-sized spherical indenters. We then calculated the contact mechanical parameters of the tissue during loading and correlated these results with the biological responses. We believe that the findings from this type of dynamic *in vitro* mechanobiological model will be useful for studying degenerative changes occurring during the early phases of OA.

2. Methods

Unless otherwise indicated, all chemicals were purchased from Thermo Fisher Scientific, Waltham, MA.

2.1 Tissue Acquisition

Skeletally mature bovine knees (>18 months) were obtained from a local abattoir within twenty-four hours of death. The intact joint capsule was opened and the femoral condyles covered with gauze soaked in phosphate buffered saline (PBS) containing 1% antibiotic/antimycotic (ab/am) to prevent drying and degradation. The condyles were then removed using an electrical saw, the condyles rinsed with PBS + 1% ab/am to remove blood and bone marrow, covered with gauze soaked in culture medium (Dulbecco's modified eagle's medium (DMEM) without phenol red, supplemented with 1% ab/am, 10 mM Hepes buffer, 1mM sodium pyruvate and 4mM L-glutamin), and stored in an incubator overnight at 37 °C for testing on the next day.

2.2 Sliding Experiments

As previously described, a condyle was mounted into a custom-designed dynamic articular cartilage test system (DACTS) [16] with a continuous flow of sterile culture medium applied to the cartilage surface for the duration of the experiment.

To obtain the curvature of the specimen, the indenter was repeatedly lowered onto the cartilage surface yielding a force-deformation response. Force in the y-direction and displacements in the x- and y-directions were recorded using a load cell and two linear variable differential transducers (LVDTs), respectively (Fig. 1A). The resulting force-deformation curve at each

location along the surface was used to calculate the surface location (at contact), which was later used to calculate the cartilage thickness after the cartilage was removed from the underlying subchondral bone. After a 20-minute recovery period the sliding protocol was applied by lowering the indenter onto the apex (x = 0) of the condyle. A 39.2 N axial force was applied and the indenter cyclically slid over the cartilage for 40 mm (x = ± 20 mm) in the x-direction at 10 mm/s sliding speed for 2000 cycles (Fig. 1). To obtain the location of the ~~true~~ cartilage surface during sliding, the coordinates of the ball center at surface contact along the path of motion were fitted using a 3rd order polynomial and used to calculate the curvature of the condyle and deformation of the cartilage, as previously described [16]. Two different-sized indenters, 17.6 mm and 30.2 mm diameter, (Delrin) were used to load the cartilage (Fig. 1B and C). Indenters were approximated from curvatures of human mandibular condylar heads (5th and 95th percentile). Immediately after 2000 cycles, full-depth cartilage specimens where removed for analyses (Fig. 1 D). Thereafter, the entire cartilage layer was removed, the bone surface mapped as described above and used to calculate the cartilage layer thickness.

2.3 Mechanical Analysis

For each loading cycle a 3rd order polynomial was fit to the deformed articular surface and corrected for curvature as described above. The initial thickness and deformation of the cartilage during the cyclic loading was calculated using a Matlab (MathWorks, Natick, MA) routine to determine the minimum distance between the cartilage surface and underlying subchondral bone. Total strain (ε) was calculated from the deformation (δ) divided by the initial thickness (l_0)

$$(\varepsilon = \frac{\delta}{l_0}). \quad (1)$$

Contact radius, maximum stress and dynamic effective modulus were calculated using Hertzian

theory of elastic deformation [23]. The contact radius (a) between the indenter and the cartilage was calculated using

$$a = \sqrt{\delta \cdot R'} \quad (2)$$

where the reduced radius (R') for the indenter (radius R_a) and condyle (radius R_b) is given by $1/R' = 1/R_a + 1/R_b$. The condyle radius was calculated from the polynomial fit to the cartilage surface given by

$$R_b = \frac{\left[1+\left(\frac{dy}{dx}\right)^2\right]^{\frac{3}{2}}}{\left|\frac{d^2y}{dx^2}\right|} \quad (3)$$

The maximum contact stress (σ_{max}) and dynamic effective modulus (E*) where then calculated at each location along the sliding path on the condyle for each individual cycle using Hertzian theory. We modeled the cartilage layer as a thin elastic compressible layer bonded to a rigid substrate (bone), which was considered incompressible. The effective modulus (E*) was calculated using

$$E^* = \frac{3 \cdot F \cdot R'^{-0.5} \cdot \delta^{-1.5}}{4} \quad (4)$$

and the maximum contact stress (σ_{max}) calculated from

$$\sigma_{max} = \frac{2 \cdot F}{\pi \cdot a^2} \quad (5)$$

both formulas for spherical indentation of a thin layer on a rigid substrate from Jaffar [24]. While the effective modulus E* is not a true material property for cartilage (it depends on several factors, such as the material properties of the cartilage and Delrin sphere, the sliding speed, deformation rate, and the reduced radius), it does provide a measure for relative changes between the different indenters in this study.

2.4 Biological Analysis

Eight knees (16 condyles) were used in this study; four were used for PG loss analysis (knee 1-4) and four for gene expression analysis (knee 5-8). For each indenter, a medial or lateral condyle was loaded, with the contralateral unloaded condyle serving as a control (Table 1). To investigate the biological response of the cartilage to the two different-sized indenters, a 5 mm cartilage specimen for histological staining was removed from the apex of the condyle immediately after loading and put in 10 % buffered formalin (Pharmco-Aaper, Brookfield, CT) + 1% cetylpyridinium chloride (Sigma-Aldrich, St. Louis, MO). In order to correlate the mechanical parameters to chondrocyte gene expression and PG loss along the loading path, ten 3 mm diameter cartilage specimens were removed from the loading path and incubated in culture medium at 37 °C as described below (Fig. 1). The specimens were collected at known locations.

2.4.1 Histology

Immediately after collection cartilage specimens were put into formalin for 3 hours, washed 3 times with tap water and stored in 70% ethanol at 4 °C for further processing. The samples were dehydrated using a gradient of ethanol from 70% to 100%, 2 steps of xylene and 3 steps of hot molten paraffin. The tissue was embedded in paraffin, cut at 5 μm thickness and mounted on a coverslip. In order to enhance attachment of the section to the glass slide, they were heated to 56°C overnight. Before staining, paraffin sections are rehydrated with 2 washes of xylene and a gradient of ethanol from 100% to 70%. As described below, sections were stained using safranin-O and picrosirius red for PG and collagen contents, respectively. Following staining, sections were rehydrated in a gradient of ethanol up to 100%, washed in xylene, air-dried, and cover-slipped using mounting medium. The sections were viewed via light microscopy with a

polarizing filter added to view the collagen structure in the picrosirius red stained sections [25]. Matrix damage in the loaded cartilage was qualitatively assessed by visually comparing the loaded cartilage histology sections to similarly prepared histology sections of healthy cartilage. No grading system was used.

Safranin-O

Sections were stained in Mayer's Hematoxylin for 7 minutes and washed in running tap water. Next, sections were counterstained in Fast Green (Sigma-Aldrich, St. Louis, MO) solution for 15 minutes, and quickly rinsed with 1% acetic acid solution for 15 seconds before staining in 0.1% safranin-O (Sigma-Aldrich) solution for 20 minutes.

Picrosirius red

Sections were stained in Fast Green for 10 minutes, transferred to 1% acetic acid for 2 minutes and quickly rinsed in tap water. Next, sections were stained in picrosirius red (Sigma-Aldrich) for 30 minutes before being rinsed in tap water.

2.4.2 Proteoglycan Loss

To investigate proteoglycan loss, medial and lateral condyles were analyzed separately. The 3 mm cartilage specimens were incubated in 700 µl culture medium at 37 °C for 48 hours. After 24 hours, medium was collected, frozen at -20 °C for further analysis and replaced with new culture medium. After 48 hours, culture medium was again collected and the cartilage specimen digested in 1 mg/mL proteinase K (MP Biomedical, Santa Ana, CA) for 16 hours at 56 °C. Digests and conditioned media samples were used to determine the proteoglycan content using the

dimethylmethylene blue (DMMB) assay [26]. The initial proteoglycan concentration of each sample was calculated by adding the loss after 24 and 48 hours to the proteoglycan measured in the tissue.

2.4.3 Gene expression analysis

Cartilage specimens for gene expression analysis were incubated in culture medium at 37 °C for 4 hours after loading was applied and subsequently frozen in liquid nitrogen for further analysis. Total RNA was extracted using the phenol-chloroform extraction method [27]. Genes for ECM proteins (aggrecan, type II collagen, fibronectin, cartilage oligomeric matrix protein (COMP)) and catabolic enzymes (MMP-3/-13 and ADAMTS-4/-5) were analyzed. Glyceraldehyde-3-phospahte dehydrogenase (GAPDH) and ribosomal protein L13a (RPL13a) were used as calibrator genes and delta–delta Ct ($\Delta\Delta$Ct) values were calculated for each gene. Forward and reverse primers for all genes used in this study can be found in Table 2.

Statistics

Average values for all measured parameters are given as the mean ± standard deviation unless otherwise indicated. To increase parameter numbers for statistical analysis, pooling of medial and lateral condyle data was performed only when no statistical differences were found (mechanical and nRNA data) by one-way ANOVA between the sampling locations, as described below and in Table 1. Two-tailed student's t-tests were used to compare the means between loaded and unloaded control groups and the two different indenters under the assumption that the variances of the populations are equal. The relationship between mechanical parameters and gene expression was assessed with univariate linear regression analysis using r-squared (r^2) to

explain the response variability and the slope of the curve to determine if the predictor is significant. The results were considered statistically significant when the significance level (α) was ≤ 0.05. Multiple comparisons were adjusted by the Tukey's range test.

3. Results

Each unloaded knee (medial or lateral control condyle) was analyzed for differences in PG loss and gene expression along the loading path, and also for differences between the knees. For each knee there were no significant differences in PG loss and gene expression found for the different sampling locations along the loading path. However, significant differences in PG loss but not for gene expression were found between controls of medial and lateral condyles (Fig. 2 and 3).

3.1 Mechanics

For each knee, the mechanical parameters for the loaded condyles did not differ along the sliding path. However differences in mechanical parameters were found between medial and lateral condyles loaded with the same indenter size (see Tables 3 and 4). Figure 4 shows the statistical analysis of mechanical parameters averaged over the sampling path (locations 1 – 10) (medial and lateral condyles were pooled only for the mechanical analysis). Sliding with the smaller 17.6 mm diameter indenter resulted in larger deformations ($p < 0.0001$), strains ($p = 0.003$) and dynamic effective moduli ($p = 0.0002$) compared to the 30.2 mm diameter indenter, while the contact radius and stress remained unaffected by indenter size. The individual mean ± standard deviations for the mechanical parameters used for correlation with the gene expression and PG loss are given in Tables 3 and 4, respectively.

3.2 Biology

3.2.1 Histology

No visual differences in Safranin-O stain intensity, a measure of PG content, was observed between loaded and control samples for either indenter. In addition, picrosirius red stained

sections, which highlight collagen when analyzed under polarized light microscopy, showed no collagen disruption at the articular surface or change in collagen alignment and orientation within the ECM between the different indenters or controls.

3.2.2 Gene Expression

No differences in gene regulation were found for control samples with respect to sampling location and between medial and lateral condyles. Therefore, controls from different locations and corresponding condyles of each indenter group were averaged (n=20) and the loaded samples normalized by the control mean values in order to get relative fold changes in gene expression (Fig. 5). Gene expressions for matrix proteins were significantly increased relative to their controls when loaded with the 17.6 mm but not with the 30.2 mm indenter. The only enzymes that were significantly up-regulated were MMP-3 and ADAMTS-5 when loaded with the 17.6 mm indenter. No difference in the gene expressions for MMP-13 and ADAMTS-4 was observed between the loaded and control samples.

A univariate regression analysis was performed between the mechanical parameters and gene expressions that were significantly affected (up-regulated) by the indenter size (Table 5). Several of the genes were found to be significantly correlated with deformation (AGG, COLL2, FN, COMP, MMP-3) and dynamic effective modulus (AGG, COLL2, FN) (Figs. 6, 7 and 8). However, only collagen type II was correlated with strain (Table 5).

3.2.3 Proteoglycan Loss (DMMB Assay)

Proteoglycan loss from the loaded and control cartilage samples was determined after 24 and 48 hours post-testing. After 24 hours condyles loaded with the 17.6 mm diameter indenter lost 7.7% (lateral) and 5.1% (medial) of the total proteoglycan, corresponding to a 1.6-fold and 1.4-

1 fold PG loss compared to the unloaded control (Fig. 2A). On the other hand, condyles loaded
2 with the 30.2 mm indenter lost 8.1% (lateral) and 5.2% (medial) of proteoglycan to the medium
3 after 24 hours (Fig. 2B). However, this loss was not different from the control condyles (1.1-fold
4 for both). After 48 hours, proteoglycan loss significantly increased only for the medial condyle
5 loaded with the smaller indenter ($p = 0.04$), all remaining samples were not different from the
6 unloaded controls (data not shown).

4. Discussion

Under reciprocating sliding conditions, contact parameters between two opposing joint surfaces depend on intrinsic (or genetic) factors, such as material properties of the cartilage and the geometry of the joint surfaces, and also external factors such as compressive forces and relative translation speed [9,10,16,28–30]. The influence of compressive forces and sliding speeds have already been investigated and deformations, contact stresses and dynamic moduli found to be functions of axial load and sliding speed [16]. The objective of the present study was to investigate the influence of joint geometry (curvature), modeled using two different-sized spherical indenters, on the mechanical and biological behavior of articular cartilage explants under reciprocating sliding load. We hypothesized that the application of a sliding load with a small diameter spherical indenter, compared to a large diameter spherical indenter, would result in increased cartilage damage, catabolic gene up-regulation and PG loss due to the increased ECM strains and stresses that arise from the reduced contact area. We found that the size of the spherical indenter indeed influences the deformational behavior of articular cartilage and unfavorable contact geometries might induce enzyme-mediated catabolic processes in the tissue.

The two opposing surfaces of a joint are never perfectly congruent, resulting in more or less favorable geometries for optimal force distribution and attenuation [18,19]. In the present study, contact parameters were calculated according to Hertz's model of elastic deformation [23] and an adjustment of the theory for elastic layers bonded to a rigid substrate (Eqns. 2, 4 and 5) [24].

Sliding with the smaller indenter (17.6 mm) resulted in higher ECM deformations than with the larger indenter (30.2 mm). This can be explained due to (1) the smaller indenter having a smaller contact area, larger contact stress and therefore greater ECM deformation, and (2) while

we used the Hertz and Jaffar models [23,24] to calculate the contact parameters, articular cartilage is not an elastic solid but rather a poroviscoelastic layer bonded to a rigid substrate (underlying bone). Therefore the subchondral bone will have a stiffening effect on the cartilage ECM that becomes more pronounced with a larger contact area, therefore restricting the total amount of ECM deformation [31]. Thus, the slightly larger contact area for the 30.2 mm diameter indenter (Fig. 4C) might explain the ~28 % higher dynamic elastic modulus (Fig. 4E) compared to the smaller indenter (17.6 mm diameter). This trend confirms earlier results from Bonnevie et al. [29] where they found a 30 % lower modulus for their 0.8 mm indenter compared to a 3.2 mm indenter.

Due to the spherical shape of the indenter the resulting contact area between the indenter and the cartilage is a function of penetration depth and curvature of the femoral condyle (Eqn. 2). In general, larger deformations with the small indenter result in similar contact radii than smaller deformations with the large indenter. In a similar manner this affects the contact stresses (Eqn. 4) and explains the insignificant differences in the contact stresses for the different indenters. This leaves ECM deformation, strain and dynamic effective modulus as the only significantly different mechanical parameters between the two indenters and these possibly are the parameters responsible for the biological differences observed (Figs. 2, 3 and 5).

The biological response of the articular cartilage to the sliding load applied by the two different indenter sizes was quantified by (1) direct damage to the ECM as visualized with histology staining, (2) changes in the chondrocyte's metabolic activity by gene expression analysis, and (3) PG loss from the ECM post-sliding. Even though the sliding contact stresses were on the high end of the physiological range [32–34], no immediate damage (PG loss and collagen fiber disruption) was observed between the loaded and control groups, or between the

two indenters. It is known that the deformational response highly depends on the parallel organization of the collagen fibers in the superficial zone of the cartilage [35–37]. Also, fluid redistribution may greatly differ in samples where a large portion of the ECM (relative to the loading area) is still intact (greater presence of interstitial fluid to shield the PGs and collagen fibers) [38]. All of these factors potentially contribute to enhanced mechanical response of larger tissue explants.

In this study condyles loaded with the 17.6 mm indenter were found to have significant up-regulation of all genes for ECM proteins compared to controls and the 30.2 mm diameter indenter. The up-regulation of aggrecan and collagen type II suggests a possible attempt by the chondrocytes to adapt the ECM to new mechanical requirements imposed by the smaller indenter, as has been well-documented in previous studies [4,39]. The up-regulation of fibronectin and COMP possibly indicates a shift from an anabolic to the catabolic gene expression as these proteins are known to be present in damaged cartilage [13,40]. Further evidence for the initiation of catabolic processes is the enhanced presence of MMP-3 and ADAMTS-5 in the cartilage loaded with the smaller indenter. While the sole up-regulation of the genes does not automatically imply enzyme synthesis (presence or activation in the ECM), it does indicate a shift in chondrocyte phenotype [41,42]. No change in the expression of MMP-13 and ADAMTS-4 was found. As it is known that gene regulation is a time-dependent process, a post-loading incubation time of 4 hours might not be enough to show up-regulation of certain enzymes [8]. Also, these enzymes could not be affected by the magnitude of loading applied in this study.

A potential indication for the presence and activation of ECM enzymes is the fact that PG loss was significantly enhanced in condyles loaded with the smaller compared to the larger indenter.

Since no direct mechanical damage was histologically observed and the synthesis for new PGs takes more than 12 days [43], it is likely that the loss of PGs detected in the culture medium was enzyme-induced.

Finally, even though contact stresses are known as major regulators of the biological response, we did not find any significant differences in contact stresses between the two indenter groups. When a regression analysis was performed between the mechanical parameters and the significantly up-regulated genes, several of the genes are significantly correlated with deformation (AGG, COLL2, FN, COMP, MMP-3) and dynamic effective modulus (AGG, COLL2, FN) (Figs. 6, 7 and 8). Only collagen type II was correlated with strain (Table 5).

This study has a few limitations that need to be taken into account and could have affected the study finding. First of all, the Delrin indenter is several times stiffer (3 orders of magnitude) than the layer of cartilage that normally articulates against the femoral condyle. As a consequence, all deformations that occur in the condyle would under *in vivo* conditions be shared (what results in larger strains and the violation of Hertz' theory). In return, this setup does model cases where one part of the joint was replaced with an artificial bearing material. Also, even though the curvatures and contact dimensions are rather small for the joints of the lower body (ankle, knee hip), they represent physiological values for the temporomandibular joint (TMJ). Second, the loading tests were conducted at room temperature which has been shown to influence gene regulation [44]. But even though basal gene regulation is temperature sensitive, it is not clear to what extent temperature affects the relative expression levels between loaded and unloaded controls.

A further limitation in our study was the use of a 10 mm/s sliding velocity. In a previous study [16] we measured the mechanical response of cartilage to different sliding velocities of 1,

2, 5, 10 and 20 mm/s. We found that an increase in sliding speed resulted in decreased cartilage deformations and strains, higher contact stresses, and increased dynamic effective modulus. The speed-dependency of these mechanical parameters was attributed to the poroviscoelastic properties of articular cartilage. In the present study we used only one speed, 10 mm/s, to avoid velocity dependent effects. Anderst and Tashman [45,46] measured peak knee contact velocities of over 100 mm/s in dogs and humans during running on a treadmill. In in vitro human knee gait simulator studies, Gilbert et al. [47] measured peak sliding velocities on the tibial plateaus as high as 100 mm/s; however over most of the stance phase the velocities were much lower, less than 25 mm/s (unpublished data, personal communication courtesy of Dr. Tony Chen). Thus our sliding speed of 10 mm/s would be representative of slower walking speeds or the slower velocity portions of the stance phase. While we did find significant differences in gene expression at 10 mm/s sliding velocity compared to controls, we cannot extrapolate these results to higher sliding velocities.

In addition, it needs to be mentioned that the assumption of independent observations for the 10 samples per condyle can be disputed as the samples are from the same condyle and therefore are correlated.

Despite these limitations, this study can be regarded as a model for investigating the effect of using different indenter curvatures on contact mechanics and consequently cartilage's metabolic response under biomimetic sliding conditions. The study clearly demonstrates that the size of the spherical indenter influences the deformational behavior of articular cartilage. Even though contact parameters were influenced to a lesser extent than hypothesized, other mechanical factors such as deformation (strain) and dynamic elastic modulus proved to affect the biological

response of cartilage under dynamic sliding conditions. The up-regulation of MMP-3 and ADAMTS-5 suggests that unfavorable contact geometries might induce enzyme-mediated catabolic processes in articular cartilage, which are common in diseases such as OA. Even taking these limitations into consideration, our results provide further understanding of cartilage contact biomechanics under dynamic migrating-load conditions. Still, further studies with greater numbers of specimens are required as the rather small number of condyles limited data analysis. Nonetheless, these results can be particularly interesting for design of prostheses where one part needs to be replaced or to surgically alleviate stress concentrations that arose after traumatic incidents such as fractures. In addition, for tissue engineering approaches it might be useful to know what contact dimensions are important to grow functional and sustainable tissue constructs.

Author Contributions

We declare that all authors contributed to the conception and design of this study and approved the submission of this manuscript. OS was responsible for data acquisition and analysis with the help of PT for interpretation of the data. PT and LG obtained funding to conduct this research and critically reviewed the manuscript.

Role of funding source

The study was supported by the Swiss National Science Foundation Grant 325230-130715 (LMG) and National Institutes of Health Grants (NIAMS) R21- AR059203 (PAT), AR 066635 (PAT) and (NCRR) C06-RR12538-01. Other than financial support, the funding sources had no role in the study design, data collection and analysis and the decision to submit the manuscript

for publication.

Conflict of interest

The authors have no potential conflicts of interest.

Acknowledgment

The authors gratefully acknowledge the support from the following funding sources: Swiss National Science Foundation Grant 325230-130715 (LMG) and National Institutes of Health Grants (NIAMS) R21-AR059203 (PAT), (NIAMS) R01AR066635 (PAT) and (NCRR) C06-RR12538-01.

References

[1] Grodzinsky AJ, Levenston ME, Jin M, Frank EH. Cartilage tissue remodeling in response to mechanical forces. Annu. Rev. Biomed. Eng. 2000;2(1):691–713.

[2] Radin EL, Burr DB, Fyhrie D. Characteristics of joint loading as it applies to osteoarthritis. In: Ratcliffe A, Woo SL-Y, Mow VC, editors. Biomechanics of Diarthrodial Joints. Springer New York; 1990. p. 437–451.

[3] Carter DR, Beaupré GS, Wong M, Smith RL, Andriacchi TP, Schurman DJ. The Mechanobiology of Articular Cartilage Development and Degeneration. Clin. Orthop. Relat. Res. 2004;427:69–77.

[4] Buschmann MD, Kim YJ, Wong M, Frank E, Hunziker EB, Grodzinsky AJ. Stimulation of aggrecan synthesis in cartilage explants by cyclic loading is localized to regions of high interstitial fluid flow. Arch. Biochem. Biophys. 1999;366(1):1–7.

[5] Jin M, Frank EH, Quinn TM, Hunziker EB, Grodzinsky AJ. Tissue shear deformation stimulates proteoglycan and protein biosynthesis in bovine cartilage explants. Arch. Biochem. Biophys. 2001;395(1):41–8.

[6] Saarakkala S, Julkunen P, Kiviranta P, Mäkitalo J, Jurvelin JS, Korhonen RK. Depth-wise progression of osteoarthritis in human articular cartilage: investigation of composition, structure and biomechanics. Osteoarthr. Cartil. 2010;18(1):73–81.

[7] Goldring MB, Marcu KB. Cartilage homeostasis in health and rheumatic diseases. Arthritis Res. Ther. 2009;11(3):224.

[8] Lee JH, Fitzgerald JB, DiMicco MA, Grodzinsky AJ. Mechanical injury of cartilage explants causes specific time-dependent changes in chondrocyte gene expression. Arthritis Rheum. 2005;52(8):2386–2395.

[9] Schätti OR, Markova M, Torzilli PA, Gallo LM. Mechanical loading of cartilage explants with compression and sliding motion modulates gene expression of lubricin and catabolic enzymes. Cartilage. 2015;6(3):185–93.

[10] Correro-Shahgaldian MR, Ghayor C, Spencer ND, Weber FE, Gallo LM. A model system of the dynamic loading occurring in synovial joints: the biological effect of plowing on pristine cartilage. Cells Tissue Organ. 2015;199(5-6):364–372.

[11] Heinegård D, Saxne T. The role of the cartilage matrix in osteoarthritis. Nat. Rev. Rheumatol. 2011;7(1):50–56.

[12] Farquhar T, Xia Y, Mann K, Bertram J, Burton-Wurster N, Jelinski L, et al. Swelling and fibronectin accumulation in articular cartilage explants after cyclical impact. J. Orthop. Res. 1996;14(3):417–423.

[13] Lohmander LS, Saxne T, Heinegård DK. Release of cartilage oligomeric matrix protein

(COMP) into joint fluid after knee injury and in osteoarthritis. Ann. Rheum. Dis. 1994;53(1):8–13.

[14] Moore AC, Zimmerman BK, Chen X, Lu XL, Burris DL. Experimental characterization of biphasic materials using rate-controlled Hertzian indentation. Tribol. Int. 2015;2–8.

[15] Lee CR, Frank E, Grodzinsky AJ, Roylance DK. Oscillatory compressional behavior of articular cartilage and its associated electromechanical properties. J. Biomech. Eng. 1981;103(4):280–292.

[16] Schätti OR, Gallo LM, Torzilli PA. A Model to Study Articular Cartilage Mechanical and Biological Responses to Sliding Loads. Ann. Biomed. Eng. 2015;1–12.

[17] Chen C, Burton-Wurster N, Lust G, Bank R, Tekoppele J. Compositional and metabolic changes in damaged cartilage are peak-stress, stress-rate, and loading-duration dependent. J. Orthop. Res. 1999;17(7):870–879.

[18] Bullough P. The geometry of diarthrodial joints, its physiologic maintenance, and the possible significance of age-related changes in geometry-to-load distribution and the development of osteoarthritis. Clin. Orthop. Relat. Res. 1980;156:61–66.

[19] Harris MD, Anderson AE, Henak CR, Ellis BJ, Peters CL, Weiss JA. Finite element prediction of cartilage contact stresses in normal human hips. J. Orthop. Res. 2012;30(7):1133–1139.

[20] Bonnevie ED, Baro VJ, Wang L, Burris DL. Fluid load support during localized indentation of cartilage with a spherical probe. J. Biomech. 2012;45(6):1036–1041.

[21] Margetson J. Rolling contact of a rigid cylinder over a smooth elastic or viscoelastic layer. Acta Mech. 1972;13(1-2):1–9.

[22] Goryacheva I, Sadeghi F. Contact characteristics of a rolling/sliding cylinder and a

viscoelastic layer bonded to an elastic substrate. Wear. 1995;184(2):125–132.

[23] Johnson KL. Contact mechanics. Cambridge University Press; 1987.

[24] Jaffar MJ. Prediction of the film thickness for the normal approach of a rigid sphere towards a thin soft layer. Tribol. Lett. 2006;22(3):247–251.

[25] Junqueira LCU, Bignolas G, Brentani RR. Picrosirius staining plus polarization microscopy, a specific method for collagen detection in tissue sections. Histochem. J. 1979;11(4):447–455.

[26] Farndale RW, Buttle DJ, Barrett AJ. Improved quantitation and discrimination of sulphated glycosaminoglycans by use of dimethylmethylene blue. Biochim. Biophys. Acta. 1986;883:173–177.

[27] Chomczynski P, Sacchi N. Single-step method of RNA isolation by acid guanidinium thiocyanate-phenol-chloroform extraction. Anal. Biochem. 1987;162(1):156–159.

[28] Moore AC, Burris DL. Tribological and material properties for cartilage of and throughout the bovine stifle: support for the altered joint kinematics hypothesis of osteoarthritis. Osteoarthr. Cartil. 2015;23(1):161–9.

[29] Bonnevie ED, Baro VJ, Wang L, Burris DL. In-situ studies of cartilage microtribology: roles of speed and contact area. Tribol. Lett. 2011;41(1):83–95.

[30] Correro-Shahgaldian MR, Colombo V, Spencer ND, Weber FE, Imfeld T, Gallo LM. Coupling plowing of cartilage explants with gene expression in models for synovial joints. J. Biomech. 2011;44(13):2472–2476.

[31] Hayes WC, Keer LM, Herrmann G, Mockros LF. A mathematical analysis for indentation tests of articular cartilage. J. Biomech. 1972;5(5):541–551.

[32] Brown TD, Shaw DT. In vitro contact stress distributions in the natural human hip. J.

Biomech. 1983;16(6):373–384.

[33] Matthews L, Sonstegard D, Henke J. Load bearing characteristics of the patello-femoral joint. Acta Orthop. Scand. 1977;48(5):511–516.

[34] Brand RA. Joint contact stress: a reasonable surrogate for biological processes? Iowa Orthop. J. 2005;25:82–94.

[35] Guo H, Maher SA, Torzilli PA. A biphasic finite element study on the role of the articular cartilage superficial zone in confined compression. J. Biomech. 2015;48(1):166–170.

[36] Korhonen RK, Wong M, Arokoski J, Lindgren R, Helminen HJ, Hunziker EB, et al. Importance of the superficial tissue layer for the indentation stiffness of articular cartilage. Med. Eng. Phys. 2002;24(2):99–108.

[37] Herzog W, Federico S. Considerations on joint and articular cartilage mechanics. Biomech. Model. Mechanobiol. 2006;5(2-3):64–81.

[38] Park S, Krishnan R, Nicoll SB, Ateshian GA. Cartilage interstitial fluid load support in unconfined compression. J. Biomech. 2003 Dec;36(12):1785–1796.

[39] Smith RL, Lin J, Trindade MC, Shida J, Kajiyama G, Vu T, et al. Time-dependent effects of intermittent hydrostatic pressure on articular chondrocyte type II collagen and aggrecan mRNA expression. J. Rehabil. Res. Dev. 2000;37(2):153–161.

[40] Barilla ML, Carsons SE. Fibronectin fragments and their role in inflammatory arthritis. Semin. Arthritis Rheum. 2000;29(4):252–65.

[41] Goldring MB, Otero M. Inflammation in osteoarthritis. Curr. Opin. Rheumatol. 2011;23(5):471–478.

[42] Kurz B, Lemke AK, Fay J, Pufe T, Grodzinsky AJ, Schünke M. Pathomechanisms of cartilage destruction by mechanical injury. Ann. Anat. 2005;187(5-6):473–485.

[43] Quinn TM, Maung AA, Grodzinsky AJ, Hunziker EB, Sandy JD. Physical and biological regulation of proteoglycan turnover around chondrocytes in cartilage explants. Implications for tissue degradation and repair. Ann. N. Y. Acad. Sci. 1999;878(1):420–441.

[44] Ito A, Nagai M, Tajino J, Yamaguchi S, Iijima H, Zhang X, et al. Culture Temperature Affects Human Chondrocyte Messenger RNA Expression in Monolayer and Pellet Culture Systems. PLoS One. 2015;10(5):e0128082.

[45] W. Anderst, R. Zauel, J. Bishop, E. Demps and S. Tashman, Validation of three-dimensional model-based tibio-femoral tracking during running, Med Eng Phys, 31 (2009), 10-16.

[46] W.J. Anderst and S. Tashman, The association between velocity of the center of closest proximity on subchondral bones and osteoarthritis progression, J Orthop Res, 27 (2009), 71-77.

[47] S. Gilbert, T. Chen, I.D. Hutchinson, D. Choi, C. Voigt, R.F. Warren and S.A. Maher, Dynamic contact mechanics on the tibial plateau of the human knee during activities of daily living, J Biomech (2013).

Figure Captions

Figure 1

(A) The Dynamic Articular Cartilage Test System (DACTS) is shown with the 39.2 N force positioned at the apex of the condyle and the load applied in the y-direction. Two different-sized indenters were used in this study (B and C). (D) The locations along the condyle loading path where biological specimens are collected for analysis after the application of the sliding load. Specimens from the corresponding unloaded control where removed from the same areas on the condyle.

Figure 2

PG loss (percent of total PG content) for each knee in loaded and control specimens after 24 hrs incubation for the (A) 17.6 mm diameter and (B) 30.2 mm diameter indenters. Each bar represents the mean ± SD (N = 10).

Figure 3

PG loss ratio (loaded/control) after 24 hours. Each bar represents the mean ± SD (N = 10).

Figure 4

Calculated mechanical parameters for the small and large spherical indenters for the last cycle of the loading phase. Each bar represents the mean ± standard deviation of four condyles with 11 sampling locations per condyle (N = 44).

Figure 5.

Relative gene expression level (loaded/control) of genes for ECM proteins: (A) aggrecan, (B) collagen type II, (C) fibronectin and (D) COMP, and catabolic enzymes: (E) MMP-3, (F) MMP-13, (G) ADAMTS-4 and (H) ADAMTS-5. Each bar represents the mean ± SD for two condyles (N = 20).

Figure 6.

Scatterplots of the regression analysis between deformation and the investigated genes (N = 40).

Figure 7.

Scatterplots of the regression analysis between strain and the investigated genes (N = 40).

Figure 8.

Scatterplots of the regression analysis between dynamic effective modulus and the investigated genes (N = 40).

Figure 1.

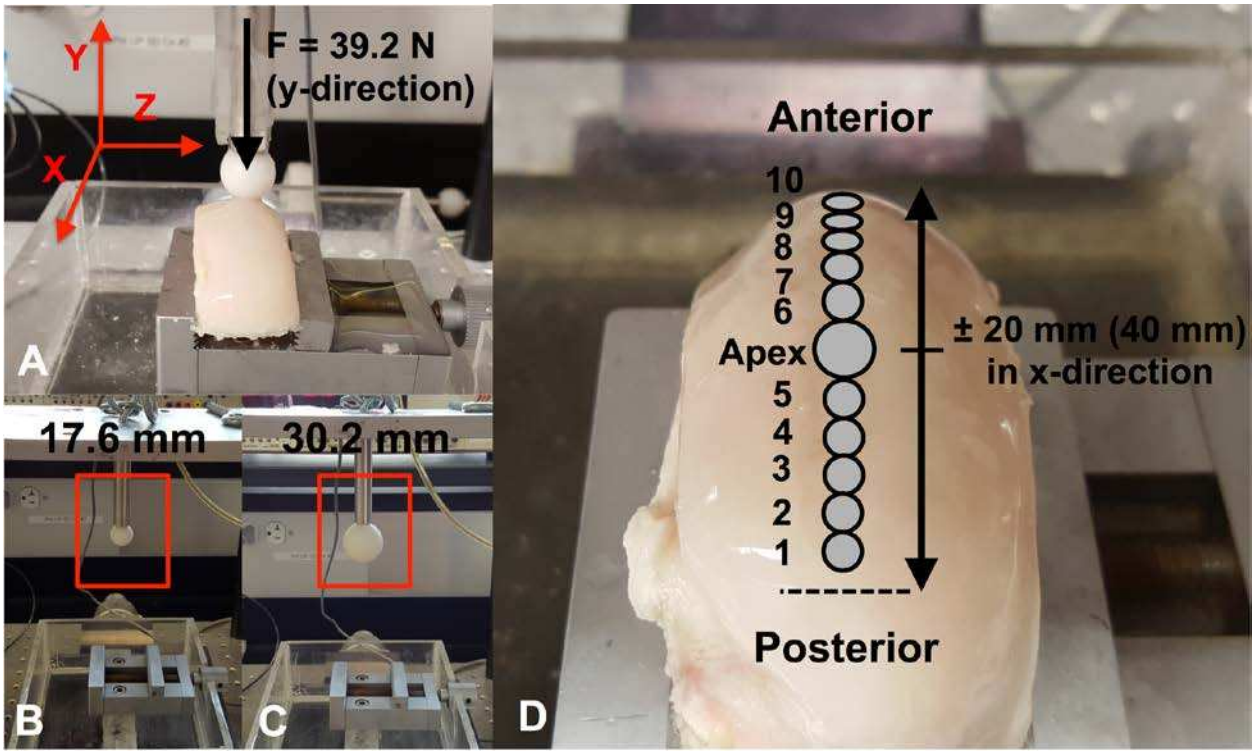
Y
Z
X
F = 39.2 N
(y-direction)
A
17.6 mm
30.2 mm
B
C
D
Anterior
10
9
8
7
6
Apex
5
4
3
2
1
± 20 mm (40 mm)
in x-direction
Posterior

Figure 2.

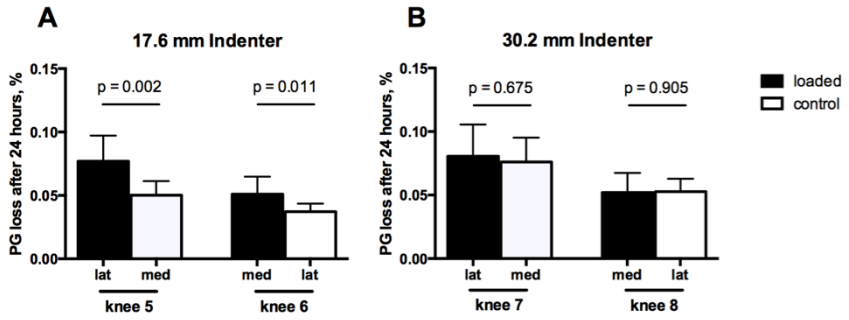
A
17.6 mm Indenter
B
30.2 mm Indenter
PG loss after 24 hours, %
0.15
0.10
0.05
0.00
p = 0.002
p = 0.011
p = 0.675
p = 0.905
loaded
control
lat
med
med
lat
lat
med
med
lat
knee 5
knee 6
knee 7
knee 8

7

Figure 3.

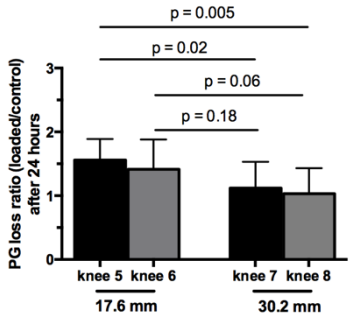
p = 0.005
p = 0.02
p = 0.06
p = 0.18
PG loss ratio (loaded/control) after 24 hours
3
2
1
0
knee 5
knee 6
knee 7
knee 8
17.6 mm
30.2 mm

Figure 4.

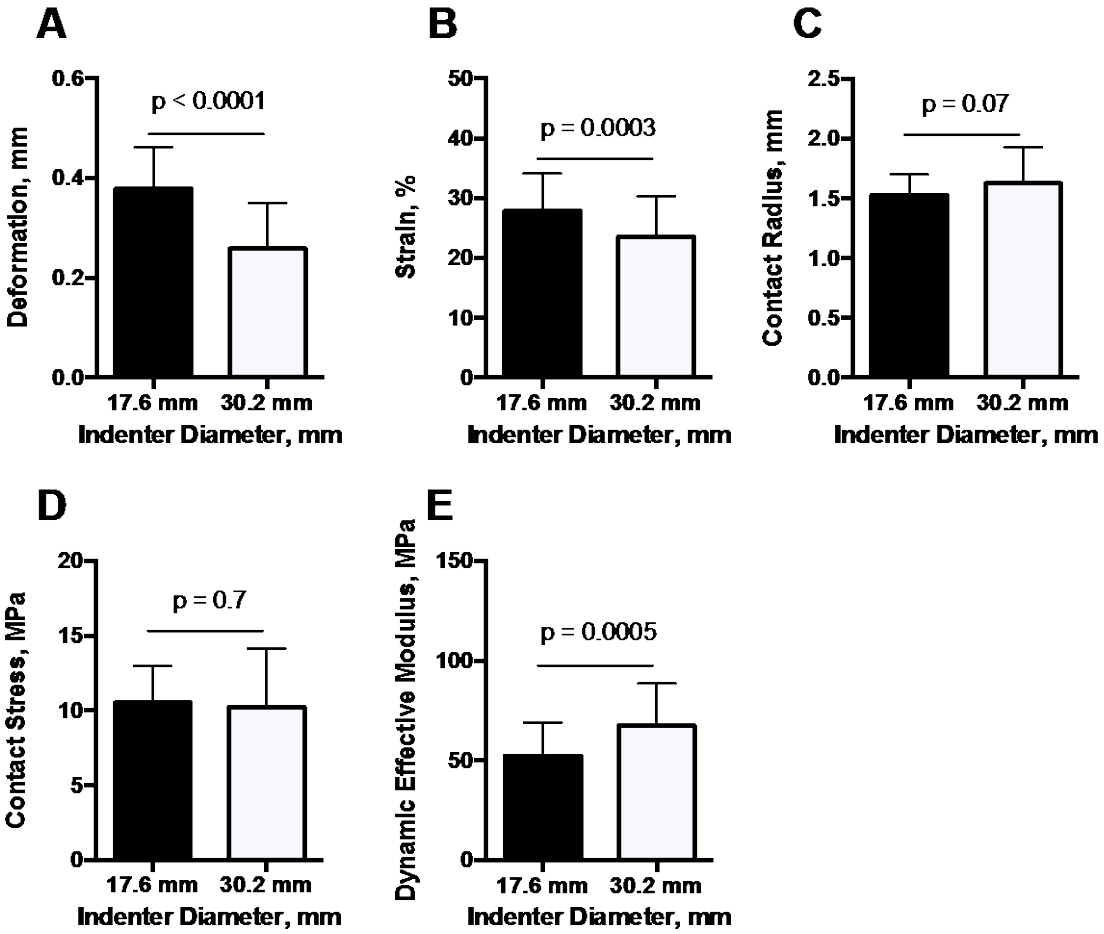
A
Deformation, mm
0.6
0.4
0.2
0.0
p < 0.0001
17.6 mm
30.2 mm
Indenter Diameter, mm
B
Strain, %
50
40
30
20
10
0
p = 0.0003
17.6 mm
30.2 mm
Indenter Diameter, mm
C
Contact Radius, mm
2.5
2.0
1.5
1.0
0.5
0.0
p = 0.07
17.6 mm
30.2 mm
Indenter Diameter, mm
D
Contact Stress, MPa
20
15
10
5
0
p = 0.7
17.6 mm
30.2 mm
Indenter Diameter, mm
E
Dynamic Effective Modulus, MPa
150
100
50
0
p = 0.0005
17.6 mm
30.2 mm
Indenter Diameter, mm

Figure 5.

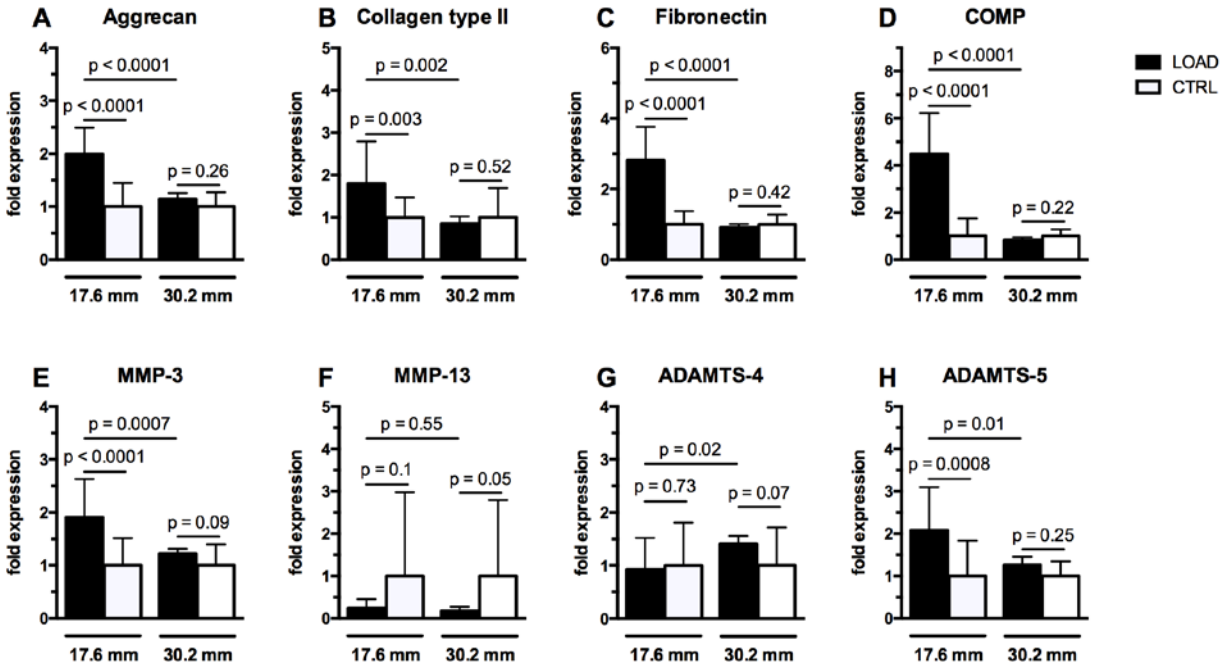
A
Aggrecan
p < 0.0001
p < 0.0001
p = 0.26
B
Collagen type II
p = 0.002
p = 0.003
p = 0.52
C
Fibronectin
p < 0.0001
p < 0.0001
p = 0.42
D
COMP
p < 0.0001
p < 0.0001
p = 0.22
E
MMP-3
p = 0.0007
p < 0.0001
p = 0.09
F
MMP-13
p = 0.55
p = 0.1
p = 0.05
G
ADAMTS-4
p = 0.02
p = 0.73
p = 0.07
H
ADAMTS-5
p = 0.01
p = 0.0008
p = 0.25
fold expression
17.6 mm
30.2 mm
LOAD
CTRL

Figure 6.

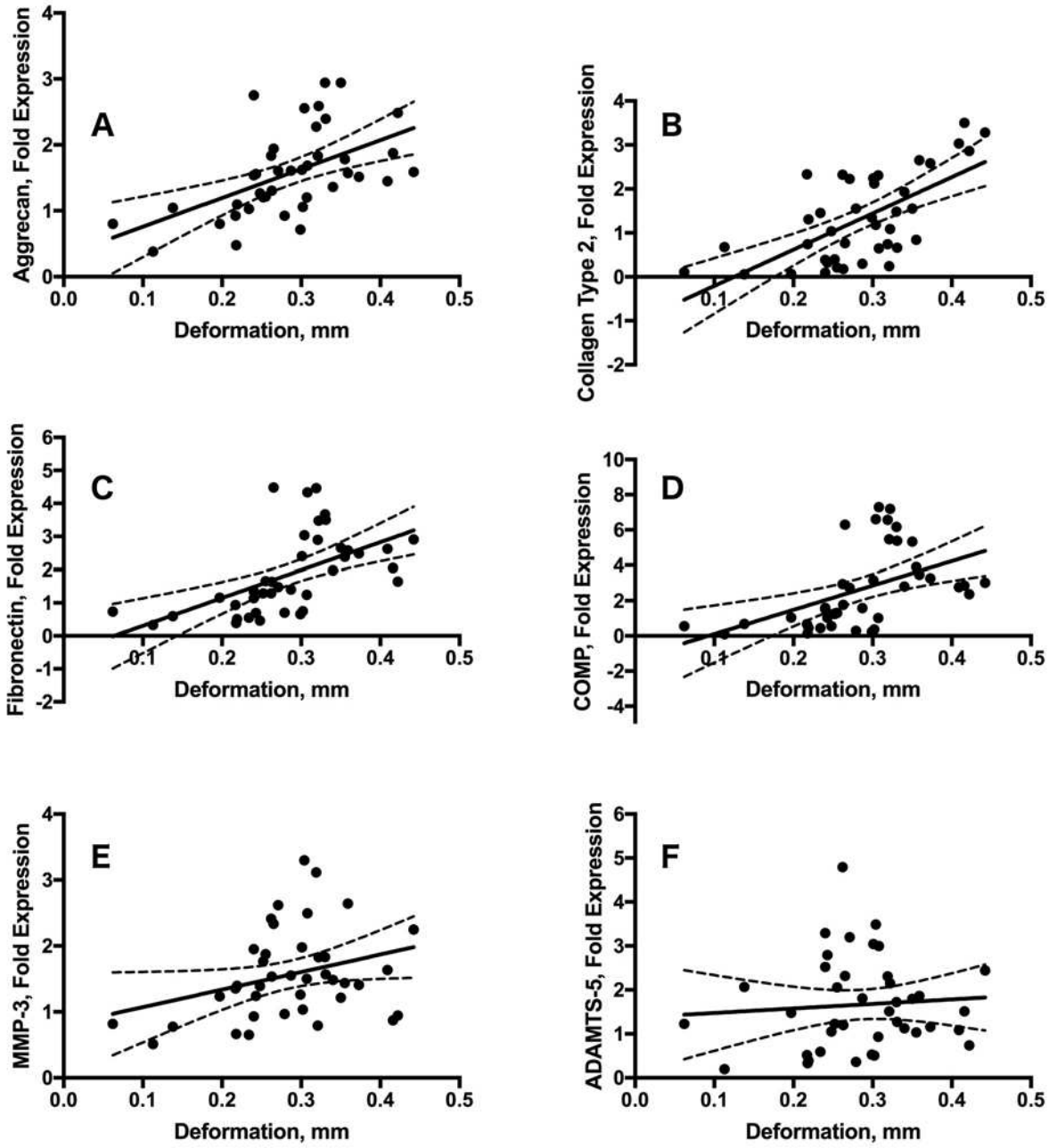
A
Aggrecan, Fold Expression
Deformation, mm
B
Collagen Type 2, Fold Expression
Deformation, mm
C
Fibronectin, Fold Expression
Deformation, mm
D
COMP, Fold Expression
Deformation, mm
E
MMP-3, Fold Expression
Deformation, mm
F
ADAMTS-5, Fold Expression
Deformation, mm

Figure 7.

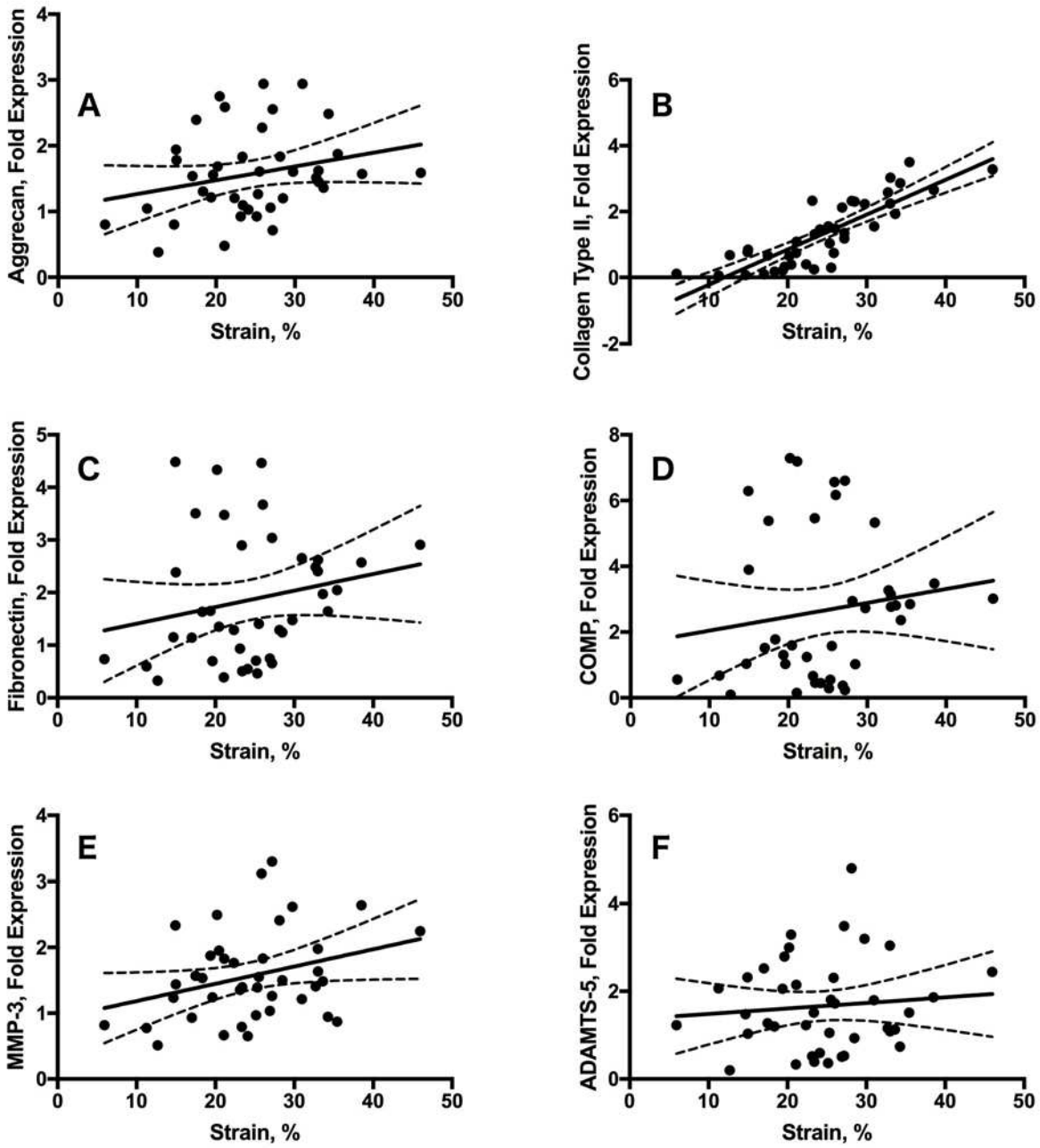
A
Aggrecan, Fold Expression
Strain, %
B
Collagen Type II, Fold Expression
Strain, %
C
Fibronectin, Fold Expression
Strain, %
D
COMP, Fold Expression
Strain, %
E
MMP-3, Fold Expression
Strain, %
F
ADAMTS-5, Fold Expression
Strain, %

Figure 8.

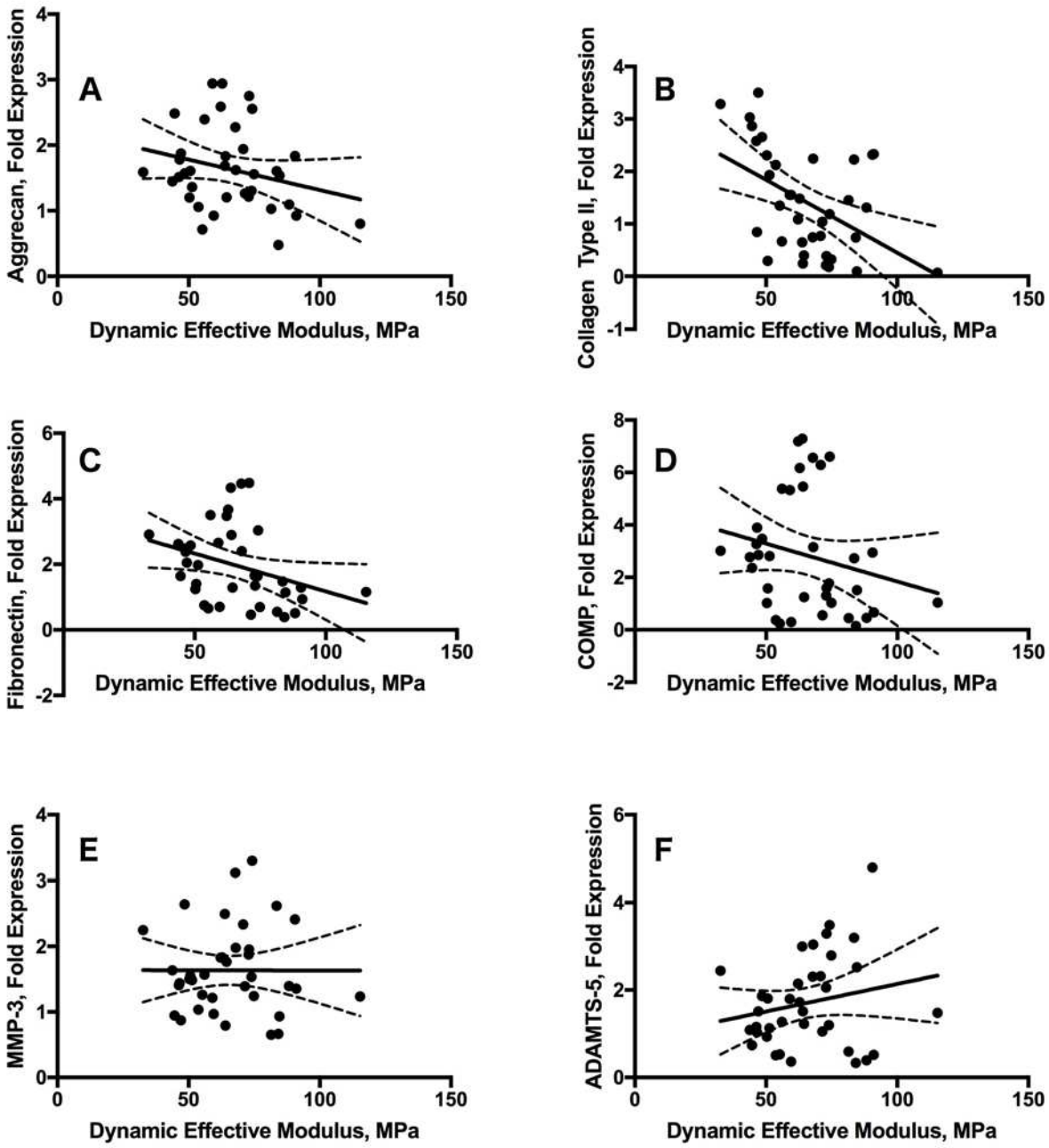
A
Aggrecan, Fold Expression
Dynamic Effective Modulus, MPa
B
Collagen Type II, Fold Expression
Dynamic Effective Modulus, MPa
C
Fibronectin, Fold Expression
Dynamic Effective Modulus, MPa
D
COMP, Fold Expression
Dynamic Effective Modulus, MPa
E
MMP-3, Fold Expression
Dynamic Effective Modulus, MPa
F
ADAMTS-5, Fold Expression
Dynamic Effective Modulus, MPa

Table 1. Sampling location and number of specimens used for pooling for different analyses

	Condyles	Indenter Radius	Sample Size	Test Used
Proteoglycan Loss 4 knees (8 condyles)	1 x loaded medial	18 mm	10	Two-tailed student's t-test (medial and lateral samples analyzed individually)
	1 x loaded lateral	18 mm	10	
	1 x control medial	18 mm	10	
	1 x control lateral	18 mm	10	
	1 x loaded medial	32 mm	10	
	1 x loaded lateral	32 mm	10	
	1 x control medial	32 mm	10	
	1 x control lateral	32 mm	10	
mRNA Analysis 4 knees (8 condyles)	2 x loaded (medial + lateral)	18mm	20	Two-tailed student's t-test (medial and lateral samples pooled)
	2 x control (medial + lateral)	18mm	20	
	2 x loaded (medial + lateral)	32mm	20	
	2 x control (medial + lateral)	32mm	20	
Mechanical Analysis 4 knees (8 condyles)	2 x medial + 2 x lateral	18 mm	44	Two-tailed student's t-test (medial and lateral samples pooled, incl. apex)
	2 x medial + 2 x lateral	32 mm	44	

Table 2: Forward and Reverse Primers

Gene	Forward	Reverse
GAPDH	GGGTCATCATCTCTGCACCT	GGTCATAAGTCCCTCCACGA
RPL13a	GCCTACTCGCAAGTTTGCCT	GCCGTTACTGCCTGGTACTT
Aggrecan	GGGAGGAGACGACTGCAATC	CCCATTCCGTCTTGTTTTCTG
Collagen II	GCTTCCACTTCAGCTATGGA	CAGGTAGGCAATGCTGTTCT
Fibronectin	CTACCCTCACGTTGTGGGAC	TTCCAGGAACTCGGAACTGT
COMP	ACCCAGACCAGCGAAATACG	ATCTGAGTTGGGCACCTTGG
MMP-3	GCAAGCCATTAAGACCACATCA	TTCTAGATATTGCTGAACAAGCTCC
MMP-13	TCCAGTTTGCAGAGAGCTACC	CTGCCAGTCACCTCTAAGCC
ADAMTS-4	CATCCTACGCCGGAAGAGTC	CATGGAATGCCGCCATCTTG
ADAMTS-5	TGGAAAGGGACGATTCGGTG	AGAGGTCAAAGACTGCCAGC

1

Table 3. Mechanical parameters from loaded condyles used for gene expression analysis

Knee #	**Condyle**	**Indenter Diameter (mm)**	**Deformation (mm)**	**Strain (%)**	**Contact Radius (mm)**	**Contact Stress (MPa)**	**Dynamic Effective Modulus (MPa)**
1	Lateral	17.6	0.31 ± 0.05	28.69 ± 8.91	1.38 ± 0.16	12.56 ± 2.65	66.37 ± 16.44
2	Medial	17.6	0.36 ± 0.04	27.97 ± 7.55	1.49 ± 0.09	10.66 ± 1.32	51.97 ± 7.43
3	Lateral	30.2	0.22 ± 0.07	17.47 ± 5.64	1.53 ± 0.26	11.50 ± 4.87	76.22 ± 18.62
4	Medial	30.2	0.24 ± 0.06	23.74 ± 4.46	1.60 ± 0.20	10.07 ± 3.27	70.58 ± 16.17

Data presented as Mean ± SD

1

Table 4. Mechanical parameters from loaded condyles used for PG loss analysis

Knee #	**Condyle**	**Indenter Diameter (mm)**	**Deformation (mm)**	**Strain (%)**	**Contact Radius (mm)**	**Contact Stress (MPa)**	**Dynamic Effective Modulus (MPa)**
5	Lateral	17.6	0.47 ± 0.08	26.23 ± 4.93	1.74 ± 0.10	7.85 ± 1.00	35.01 ± 8.49
6	Medial	17.6	0.36 ± 0.06	27.57 ± 3.79	1.51 ± 0.11	10.56 ± 1.64	54.03 ±13.00
7	Lateral	30.2	0.33 ± 0.13	30.60 ± 5.83	1.88 ± 0.40	7.95 ± 3.42	60.45 ± 38.80
8	Medial	30.2	0.23 ± 0.07	21.78 ± 4.92	1.46 ± 0.21	12.04 ± 4.04	76.84 ± 25.08

Data presented as Mean ± SD

Table 5. Univariate regression analysis between mechanical parameters and gene expression that were significantly affected by indenter size. R-squared explains the response variability while the p-value determines the significance of the predictor (N = 40).

		Aggrecan	Collagen Type II	Fibronectin	COMP	MMP-3	ADAMTS-5
Deformation	Equation	Y = 4.378*X + 0.3195	Y = 8.248*X - 1.032	Y = 8.406*X - 0.5348	Y = 13.74*X - 1.266	Y = 2.663*X + 0.8048	Y = 1.028*X + 1.373
	Slope (95% CI)	2.098 to 6.658	5.107 to 11.39	4.271 to 12.54	5.657 to 21.82	0.005344 to 5.32	-3.247 to 5.302
	R square	0.28	0.43	0.31	0.24	0.10	0.01
	P-value	0.0004	<0.0001	0.0002	0.0014	0.049	0.63
Strain	Equation	Y = 0.02098*X + 1.055	Y = 0.1058*X - 1.267	Y = 0.03149*X + 1.093	Y = 0.04222*X + 1.621	Y = 0.02626*X + 0.9221	Y = 0.01254*X + 1.359
	Slope (95% CI)	-0.004957 to 0.04692	0.08349 to 0.1281	-0.01692 to 0.0799	-0.04888 to 0.1333	-0.0002224 to 0.05275	-0.02996 to 0.05503
	R square	0.07	0.71	0.04	0.02	0.10	0.01
	P-value	0.11	<0.0001	0.20	0.35	0.05	0.55
Dynamic Effective Modulus	Equation	Y = -0.009296*X + 2.246	Y = -0.0278*X + 3.23	Y = -0.02317*X + 3.491	Y = -0.02889*X + 4.73	Y = -7.241e-005*X + 1.639	Y = 0.0126*X + 0.8798
	Slope (95% CI)	-0.02154 to 0.002951	-0.04543 to -0.01016	-0.04579 to -0.0005516	-0.07287 to 0.01508	-0.01328 to 0.01313	-0.008072 to 0.03327
	R square	0.06	0.23	0.11	0.05	0.00	0.04
	P-value	0.13	0.003	0.04	0.19	0.99	0.22